

RESEARCH

Open Access



Development of Live Load Distribution Factor Equation for Concrete Multicell Box-Girder Bridges under Vehicle Loading

Won Choi¹, Iman Mohseni¹, Jongsup Park² and Junsuk Kang^{1,3*}

Abstract

The evaluation and design of concrete bridges in large part depend on the transverse distribution characteristics of the live load carried and the service level. The live load distribution for continuous concrete multicell box-girder bridges varies according to bridge configuration, so when designing such bridges, it is important to determine the maximum negative stress at the piers, the midspan positive (tensile) stress and the deflection of the bridge when subjected to live loads. This paper reports an extensive parametric study to determine the maximum stress, deflection, and moment distribution factors for two span multicell box-girder bridges based on a finite element analysis of 120 representative numerical model bridges. Bridge parameters were selected to extend the parameters and ranges of current live load distribution factors defined by AASHTO LRFD specifications. The results indicate that the span length, number of boxes, and the number of lanes all significantly affect the positive (tensile) and the negative (compression) stress distribution factors. A set of equations proposed to describe the behavior of such bridges under AASHTO LRFD live loads yielded results that agreed closely with the numerically derived results for the stress and deflection distribution factors.

Keywords: finite element modelling, distribution factor, truck, box bridges

1 Introduction

Concrete multicell box-girder (MCB) bridges are commonly used for highway bridges in road networks all over the world. Voids are created in girders to reduce their weight, creating bridges that combine excellent torsional stiffness with elegance (Song et al. 2003). Accurately calculating the design stress and deflection actions for a multicell box-girder bridge under service loads can be a complex task, however. The design stresses and deflection demands for an individual box depend on a number of parameters, including the position of the live loads, the web spacing, the span length, and the relative deck-to-girder stiffness. To simplify the design process,

a long-standing methodology has evolved in which a multiple girder bridge deck is treated as a one-girder line or beam element (Semendary et al. 2017; Samaan et al. 2002b). Early live load distribution factors were obtained based on the method proposed by Newmark (1938), which over time has been updated as improved bridge analysis methods have become available. The concept of a live load distribution factor (*LDF*) was first used in the bridge specifications issued by the American Association of State Highway Officials (AASHTO) in 2002 through empirical *S/D* expressions (known as *S-over* equations), where *S* is the girder spacing and *D* is a constant that depends on the bridge's superstructure and the type of lane loading. *S-over* equations were used for bridge design for over a decade until the 8th edition of AASHTO's *LRFD Bridge Design Specifications* (2017) was published.

An extensive study on bridges constructed using prestressed concrete girders, steel girders and T-beams

*Correspondence: windkplus@hotmail.com; junkang@snu.ac.kr

¹ Department of Landscape Architecture and Rural Systems Engineering, Seoul National University, 1 Gwanak-ro, Gwanak-gu, Seoul 08826, South Korea

Full list of author information is available at the end of the article
Journal information: ISSN 1976-0485 / eISSN 2234-1315

(Hays et al. 1986) indicated that neglecting the effect of span length of bridges on *LDF* produces unconservative values for short span bridges and uneconomical designs for medium size bridges. Given the increasing demand for highway bridges, several researchers have sought to develop new equations for *LDFs* that take into account shear and bending moments (Huo et al. 2003; Zokaie et al. 1993; Bae and Oliva 2012; Terzioglu et al. 2017). The *LDF* formulae presented in the latest edition of the AASHTO *LRFD Bridge Design Specifications* (2017) are based on extensive numerical and field tests performed on bridges with various geometries (Zokaie et al. 1993), but their accuracy has not been reevaluated in the light of recent research in this area. In addition, these specifications do not provide sufficient details to justify and confirm the accuracy of the modification factor for continuity that has been proposed (Samaan 2004; Barr et al. 2001; Higgins et al. 2011; Hughs and Idriss 2006). At present, the following equation is generally used to derive the *LDF* for each bridge girder (Fanous et al. 2010):

$$LDF_i = N_L \frac{L_i}{\sum_{i=1}^n L_i} \tag{1}$$

where LDF_i =live-load distribution factor of the *ith* girder; L_i =moment or deflection of *ith* girder, $\sum L_i$ =sum of all girder actions; and n =number of bridge girders (bridge webs in box-girder bridges).

AASHTO LRFD (2017) adopted the proposed equation by Zokaie et al. (1993) for live load distribution factors of multicell box-girder bridges with two or more lane loading as follows:

$$LDF_m = \left(\frac{13}{N_c}\right)^{0.3} \left(\frac{S}{5.8}\right) \left(\frac{1}{L}\right)^{0.25} \tag{2}$$

where N_c and S are the number of boxes and width of each box, respectively, and L denotes the span length of bridge. Although various equations have been proposed (Zokaie 2000; Samaan et al. 2002a; Huo and Zhang 2008) cover a wide range of bridge geometries and are necessarily simplified, because of the limited number of cases examined, these equations must be modified for use under real world traffic conditions (Mohseni and Khalim 2013; Deng et al. 2017; Deng and Phares 2016). This paper

presents the results of parametric studies conducted on 120 continuous two and three span MCB bridges. The parameters that have been varied are the span lengths, the number of boxes, and the number of traffic lanes. The resulting empirical equations were determined based on a statistical analysis and the elastic response of each bridge for the standard AASHTO (2014) truck loading in order to estimate the live load distribution across a bridge. Statistical analyses were performed using best-fit technique of least squares method adopted from the NCHRP rep. 12–26 (Zokaie et al. 1993).

2 Objectives

The main objective of this study was to evaluate the *LDFs* for concrete MCB bridges with two equal spans under vehicle loads using finite element analysis (FEA). One-hundred twenty numerical models were analyzed to: (a) determine the influence of each of the parameters affecting the prototype bridge responses; (b) produce a database for negative (compression) and positive (tensile) distribution factors corresponding to the AASHTO (2014) live loads; and (c) develop a set of empirical equations for a bridge’s stress and deflection distribution factors under AASHTO-LRFD live loads. As previous sensitivity studies revealed that changing the slab thickness has an insignificant effect on the live load distribution factors (Huo et al. 2003; Huo and Zhang 2008), only the following parameters were investigated in this study: the span length, the number of lanes and the number of boxes. The superstructure is idealized using the following assumptions: (a) all materials are elastic and homogeneous; (b) the slab has a constant thickness; (c) the slab and girder exhibit full composite action; (d) the effects of the curbs and web slope are ignored; and (e) the skew angle of the bridges is less than 30°.

3 Geometric and Structural Properties

One hundred twenty MCB bridges were modeled for this study. The bridges were simply supported with two continuous equal spans of varying length. Table 1 shows the cross sectional configurations obtained for a span-to-length ratio of 24, which has been shown to be the most economical arrangement (Hall et al. 1999). The bridges were designed and optimized using CSIBridge software based on the AASHTO LRFD (2017) bridge design

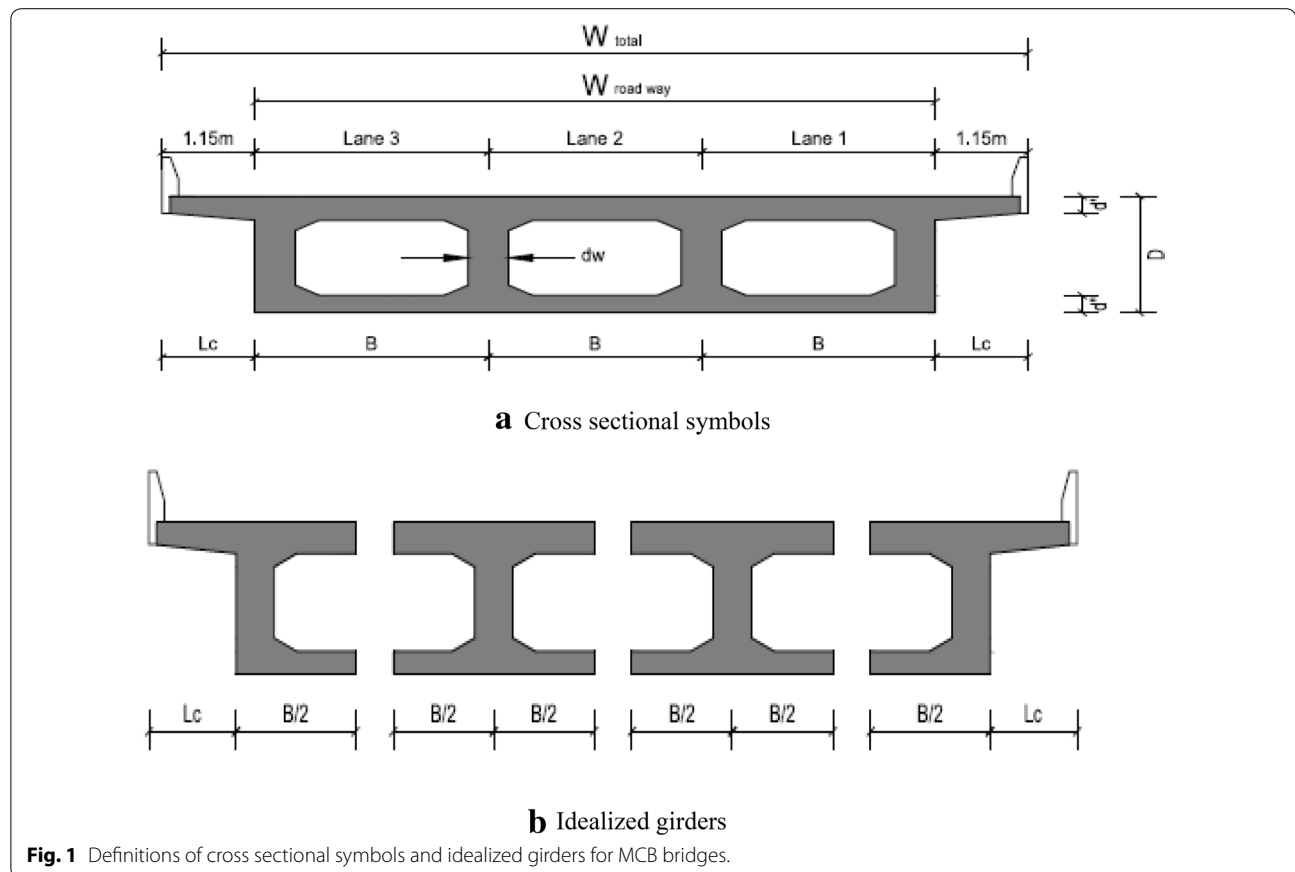
Table 1 Geometry of the bridges used in the parametric study (unit: m).

Set	L (m)	N_B	N_L	W_r	W_{Total}	d'	d''	d_w	L_c
1	(30.5, 45.75, 61, 76.25, 91.50)	2, 3	1, 2	9.10	13.00	0.20	0.15	0.10	0.61
2		2, 3, 4	1, 2, 3	14.0	16.70	0.20	0.15	0.10	1.20
3		3, 4, 5, 6	2, 3, 4	17.1	24.00	0.20	0.15	0.10	1.45

specifications. Figure 1 provides a visual representation of the definitions of the cross sectional symbols W_{total} (the total width of the bridge), W_r (the width of the roadway of the bridge), L_c (the length of the cantilever), d' (the thickness of the top flange), d'' (the thickness of the bottom flange), N_B (the number of boxes), B (the width of the boxes), D (the depth of the boxes) and L (the length of the span) used in Table 1. In order to cover a wide range of bridge spans, five different lengths ranging from 30.5 to 91.5 m were considered. It should be noted that a large number of highway bridges constructed in the US during the past decades had span lengths between 75 to 90 m. Bridges carrying two, three and four lanes of traffic (N_L) were considered in this study; the total bridge width was taken to be 9.1 m for two traffic lanes, 14.0 m for three lanes and 17.1 m for four traffic lanes. Practical ranges were selected based on Zheng's (2008) study of the box girders in box-girder bridges. For all the bridges used in these parametric studies, the modulus of elasticity of the concrete (E_c), Poisson's ratio (ν_c) and weight per unit volume were 22.80 GPa, 0.20, and 23.6 KN/m, respectively. The modulus of elasticity (E_s) and Poisson's ratio of steel (ν_s) were 200 GPa and 0.3, respectively. The top and bottom slab thicknesses were 20 cm and 15 cm, respectively.

4 Bridge Prototype Modeling

The commercially available finite element program, CSI-bridge version 20 Computers & Structures, Inc. (2017), was used in this study to evaluate the structural behaviors of MCB bridges; prototype model properties defined parametrically are the layout reference line, spans, and support conditions. In this study, the prototype bridges are modeled using a four node, three-dimensional shell element with six degrees of freedom at each node. The top and bottom shell element of the webs are integrated with the top and bottom slab at connection points to improve the compatibility of the deformations obtained (Mohseni et al. 2014). The bridge modeling was verified by comparing the live load distribution factor (LDF) derived from field tests with those from the method adopted here. Boundary conditions were simulated as being hinge-bearing at the beginning abutment and roller-bearing for all other supports. Figure 2 shows a finite element model of a 61 m three-box multicell box-girder bridge. The results of two study were used to verify the finite element modeling method used in this study.



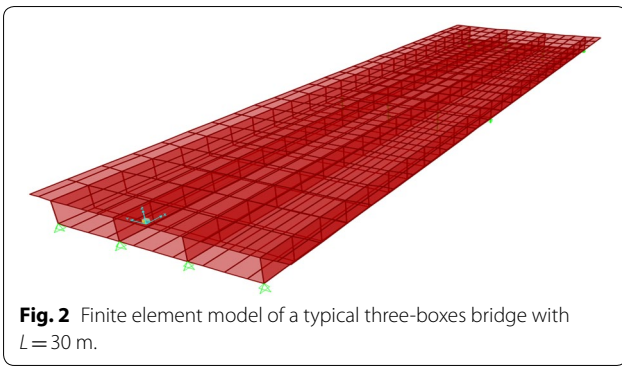


Fig. 2 Finite element model of a typical three-boxes bridge with $L = 30$ m.

4.1 Field-Testing Study on Tsing Yi South Bridge

The results of a field test study conducted by Ashebo et al. (2007) were employed to verify the results of finite element modeling technique using SAP2000 software. The duplicated Tsing Yi South Bridge in the New Territories west in Hong Kong was selected for this study. The bridge is a three-span continued structure with a skew angle of 27°, total length of 73 m, and two lanes with a carriage-way. The modulus of elasticity and weight of concrete are 26 GPa and 24.5 GPa, respectively. The bridge configuration and boundary conditions are presented in Fig. 3.

The modal test was mainly conducted to obtain the dynamic responses of the bridge such as the fundamental frequencies and the mode shapes. The technique

adopted in this study was the ambient vibration test. The dynamic responses of the bridge subjected to controlled traffic conditions were also evaluated. Table 2 tabulated the results obtained from three experimental modal tests as well as those obtained from randomly selected controlled traffic. The analytical results from 3-D FEA of the selected bridge were also taken from Ashebo et al. (2007). To verify the adopted bridge modeling method, the fundamental frequencies of the selected bridge obtained from CSIbridge were presented in Table 2. The bridge was meshed with 396 four-node shell elements. It was observed that the results from CSIbridge were in good agreements with field test results so that for most cases the modeling method of this study obtained more compatible results than those of analytical method by Ashebo et al. (2007).

Figure 4 shows the comparison of the experimental and numerical mode shapes and first fundamental frequency. It can be seen that the first mode shape from field tests was 6.5% higher than that from CSIbridge. The *LDF* and dynamic load allowance (DLA) from experimental study were 1.24 and 0.24, which had good agreements with 1.26 and 0.26, respectively, from FEA. It, therefore, was proved that the finite element models adopted in this study could reliably simulate the responses of multicell box-girder bridges.

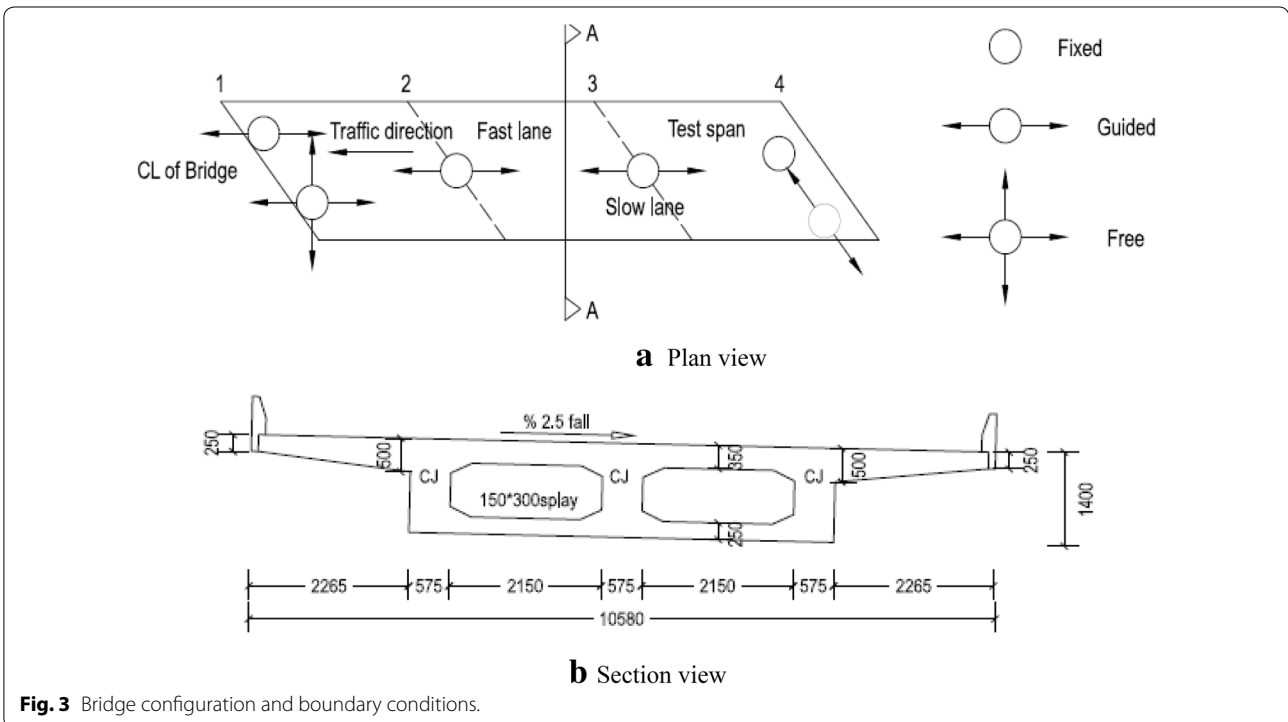
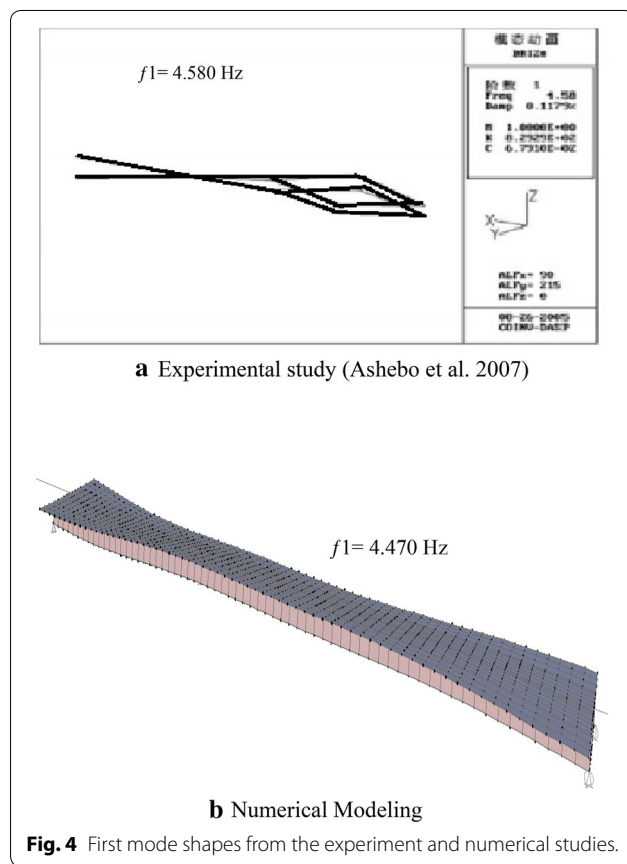


Fig. 3 Bridge configuration and boundary conditions.

Table 2 Comparison between field test and FEA.

Mode number	1	2	3	4	5	6	7	8
Ashebo et al. (2007)								
SAP2000	4.54	4.81	6.70	7.53	10.40	10.78	14.72	16.34
Field test								
1st	4.46	*	6.25	7.82	*	10.87	13.67	15.74
2nd	4.61	*	6.22	7.73	*	10.81	13.30	15.74
3rd	4.58	*	6.39	7.76	*	11.11	13.31	15.73
Control traffic	4.58	*	6.15	*	*	*	*	*
CSIbridge	4.47	4.88	6.45	7.62	10.22	11.07	14.33	16.03

* Means undetermined values in field-testing.



4.2 Scaled Two-box Bridge Under Concentrated Loads

Li (1992) presented the experimental studies on a scaled two-span box-girder bridge subjected to self-weight and concentrated loads at mid-span, which were used to verify the modeling methodology adopted in this study. The plan view and cross-section of bridge are shown in Fig. 5. The solid end diaphragms were installed at abutments and piers, and loaded eccentricly over the outer webs. Figure 6 shows the comparison between distributions of stress and deflection for selected bridges obtained from

Li’s study, CSIbridge software, and conventional beam theory.

5 Loading Conditions

This study adopted the HL-93 truck loading designated in the AASHTO LRFD (2017) (Fig. 7). The HL-93 design truck consists of a design truck plus design lane load or design tandem plus design lane load, whichever induces the worst case. For the finite element modeling, as many truck as possible were located on a bridge’s superstructures in the transverse direction based on the number of lane loaded. Maximum positive (tensile) stress and deflection were evaluated for the addition of each truck, side-by-side, and finally the maximum values were obtained (Zokaie 2000). Figure 8 shows the HL-93 truck loading cases in the transverse direction of bridge to find the critical loading configurations.

The combination of 90% of two trucks spaced a minimum distance of 15.20 m apart plus 90% lane load was used in this study to obtain the negative (compressive) stress at the piers of bridges based on AASHTO LRFD (2017) specifications (Fig. 9). The AAHTO LRFD vehicular live loads are available in the library of the CSIbridge software. Based on the AASHTO LRFD specifications, multiple presence factors of 1.00, 0.85 and 0.65 for two, three, and four lane loading, respectively, were also applied in this study.

6 Live Load Distribution Factor (LDF)

The MCB cross section was modelled as an equivalent I-beam with the same size and web properties as those commonly used in MCB bridges, as shown in Fig. 1b, with each equivalent girder consisting of one web and its associated top and bottom concrete flanges. To calculate the distribution factors for the maximum positive stresses, $D\sigma_{po}$, and negative stresses, $D\sigma_{ne}$, the two continuous equal span model girders were loaded with the total AASHTO LRFD live loads to produce the maximum positive moment, M^+ , near the midspan and the maximum negative moment,

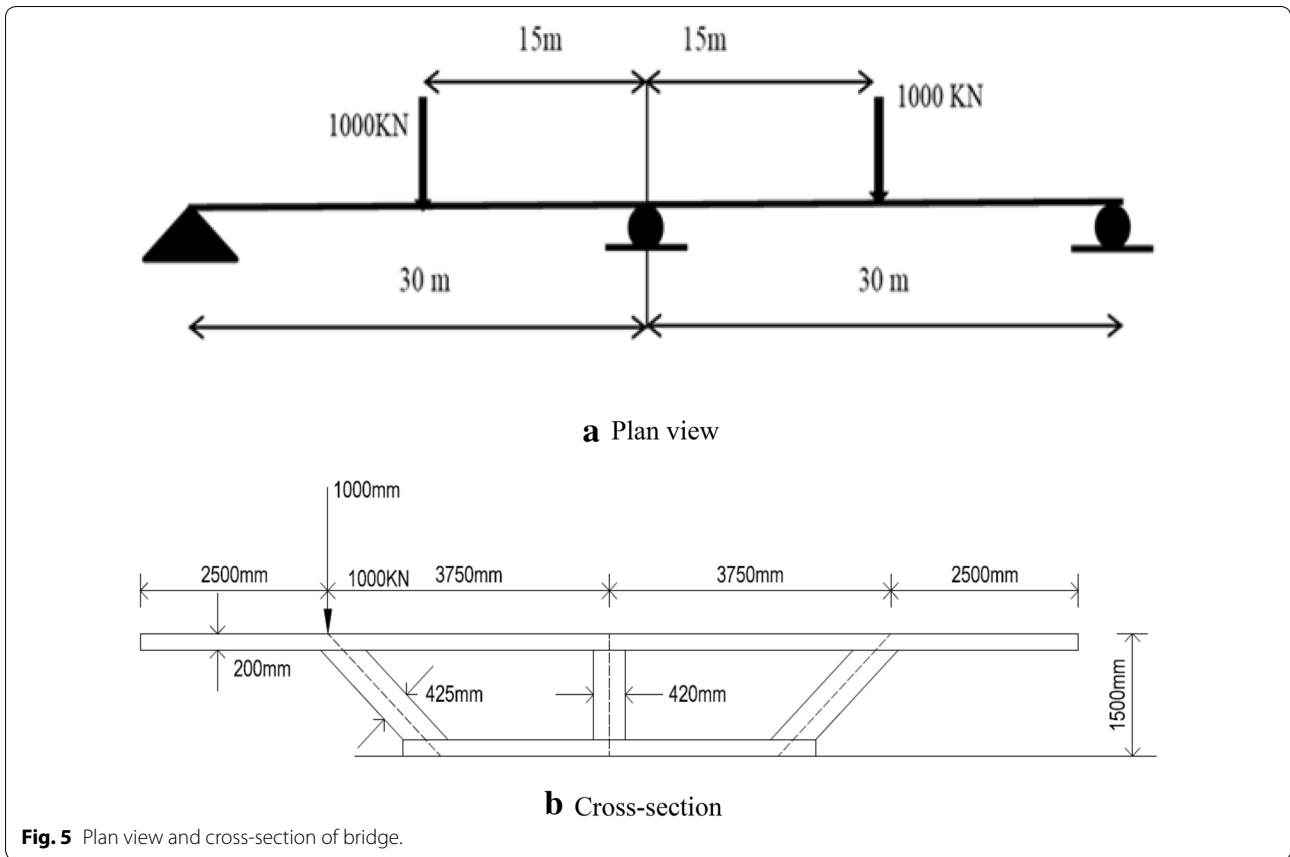


Fig. 5 Plan view and cross-section of bridge.

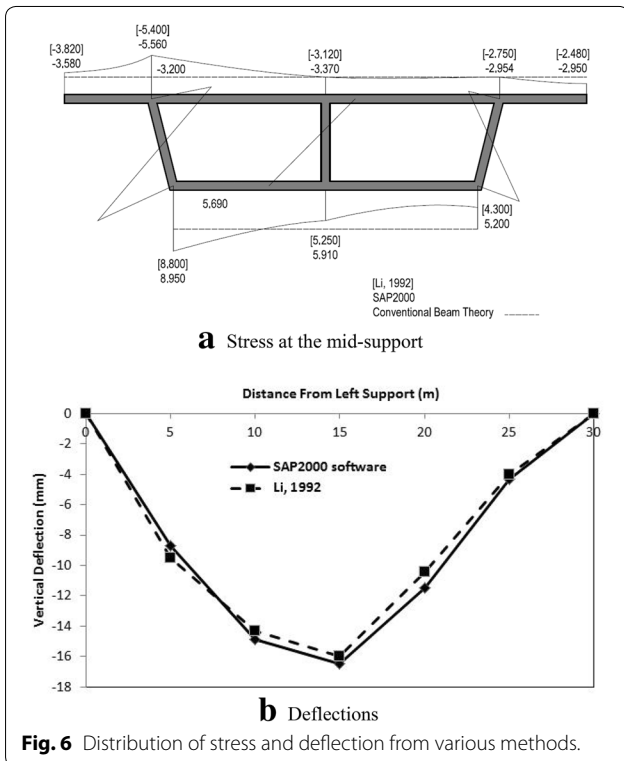


Fig. 6 Distribution of stress and deflection from various methods.

M , at the interior support. The maximum positive (tensile) stress, $\sigma_{p,I}$, and negative (compression) stress, $\sigma_{n,I}$, at the bottom fiber were calculated using a simple beam bending formula. The maximum positive (tensile) stress, σ_p , and negative (compression) stress, σ_n , for the bridges were then obtained for the three-dimensional bridges using FEA. The resulting distribution factors for positive (tensile) and negative (compression) stress were calculated as follows:

$$D\sigma_{po} = \frac{\sigma_p}{\sigma_{p,I}} \tag{2}$$

$$D\sigma_{ne} = \frac{\sigma_n}{\sigma_{n,I}} \tag{3}$$

The distribution factor for maximum deflection was calculated in the same manner as that used for maximum stress. The maximum deflections, δ_{max} , for the bridges were obtained directly from FEA. The simple ideal girder was loaded to determine the maximum deflection, δ_s , at the midspan, giving the distribution factor for maximum deflection, $D\delta_s$, in a continuous sophisticated bridge as:

$$D\delta_s = \frac{\delta_{max}}{\delta_s} \tag{4}$$

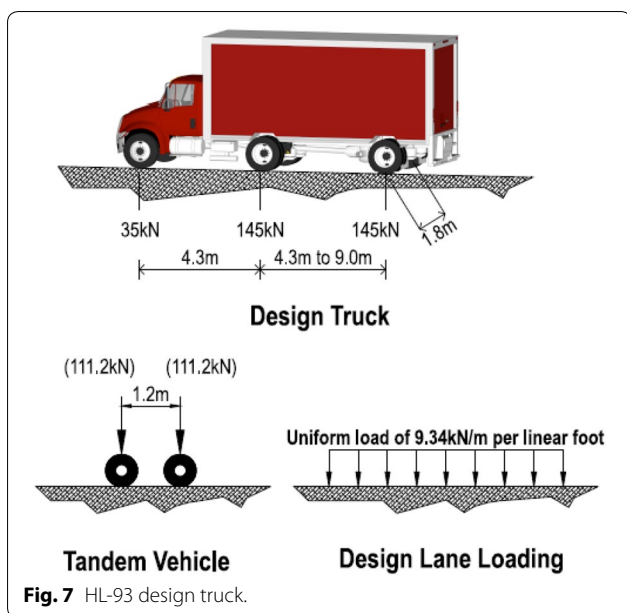


Fig. 7 HL-93 design truck.

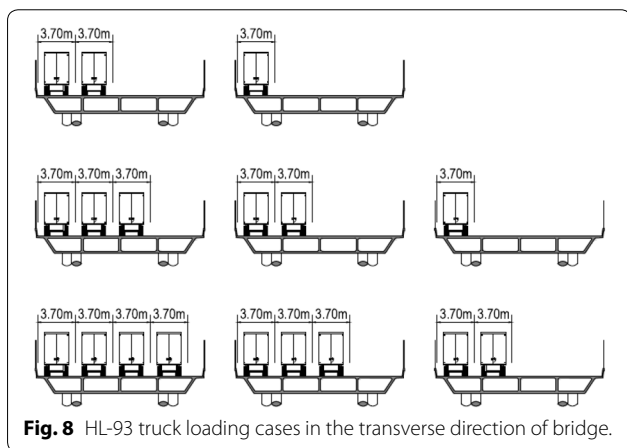


Fig. 8 HL-93 truck loading cases in the transverse direction of bridge.

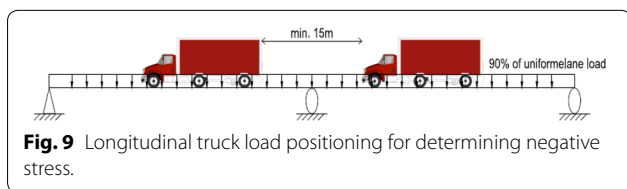


Fig. 9 Longitudinal truck load positioning for determining negative stress.

7 Discussion of Results

Parametric studies were performed on straight MCB bridges ($\theta = 0$) with two continuous spans. The live load stress and deflection distribution factors were obtained using FEA for various types of MCB bridges. The effects of various structural parameters on stress and the deflection distribution factors were investigated to identify the parameters affecting the load distribution

factors under live loads. The following results were obtained.

7.1 Effect of the Number of Boxes

The relationship between the number of boxes (N_B) and the stress distribution factors is shown in Fig. 10. The results reveal that both $D\sigma_{po}$ and $D\sigma_{ne}$ decreased as N_B increased. For instance, $D\sigma_{po}$ increased from almost 27% to 32% when N_B went up from three to four. The effect of N_B was more significant when the span lengths were shorter. The effect of N_B on the deflection distribution factors is shown in Fig. 11a. Here, $D\delta_s$ decreased as the number of box increased, by up to 32% for bridges with a span length of 60 m. The same trend is also visible for bridges with other span lengths.

7.2 Effect of the Number of Lanes

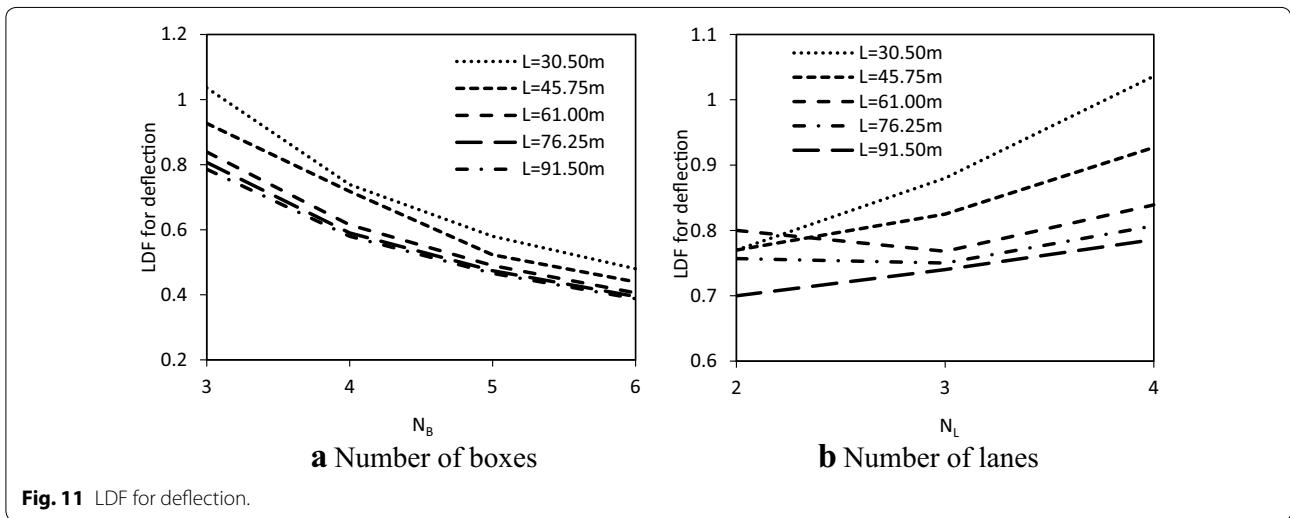
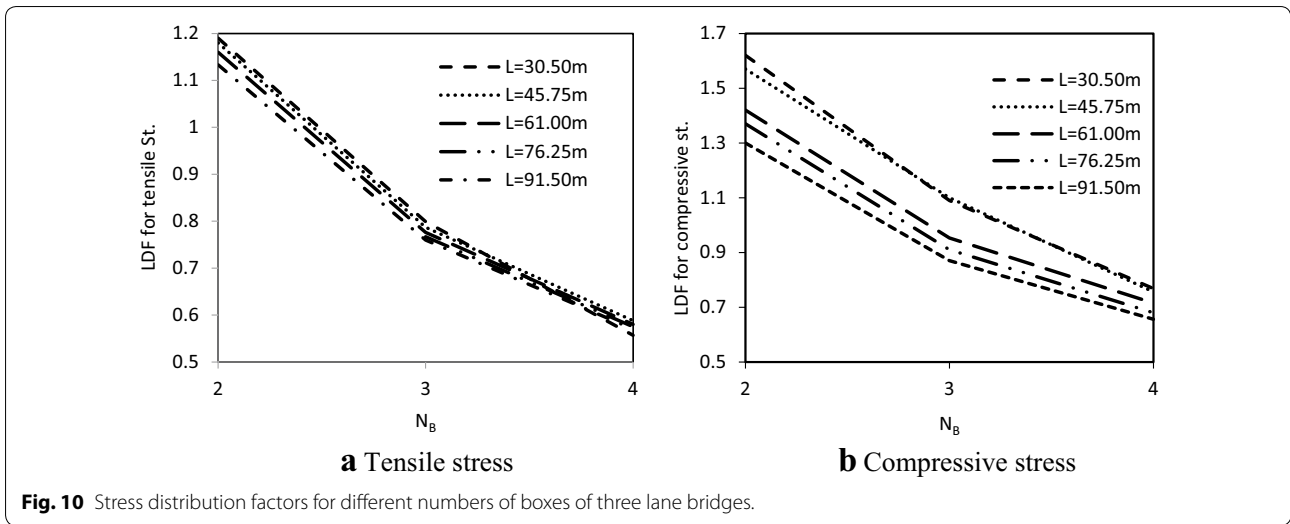
The results obtained for different numbers of lanes (N_L) are shown in Figs. 11b and 12. Here, as the number of lanes increased the *LDFs* for tensile and compression stress and deflection also increased, even after accounting for the modification factor applied due to multiple-lane loading. The stress distribution factors increased by almost 23% when the number of lanes rose from two to three.

7.3 Effect of Span Length

As the span length increases, the distribution factors for maximum positive (tensile) stresses increase but those for negative (compression) stresses decrease as shown in Figs. 10 through Fig. 12. For instance, it is shown from Fig. 12 that the increment of the span length from 30.5 to 91.5 m decreased *LDFs* for tensile and compressive stresses by up to 11% and 33%, respectively. Similarly, the *LDFs* for deflection also decreased as the span length of bridges increased. As shown in Fig. 11, *LDFs* for deflection decreased with increasing the span length from 45.75 to 91.5 m by 15%.

7.4 Comparison of Analytical Results with Current Specifications

The analytical results obtained for both the positive (tensile) and negative (compression) stresses for a bridge with a span length of 60 m were compared with those given by the LFRD formulas and AASHTO standards specifications (Fig. 13). Interestingly, the distribution factors for tensile stresses obtained from FEA were significantly smaller than those calculated using the current AASHTO (2002) standard and AASHTO LFRD (2017) specifications by 33% and 46%, respectively. Current AASHTO standard and specifications, therefore, provide highly conservative values for tensile stress distributions on bridge superstructures. In the case of



compressive stresses, the differences between FEA and AASHTO were reduced. The live load distribution factors calculated using FEA were higher than those from the LRFD formulas (Eq. (2)) by 13%, but they were still smaller than those obtained from the AASHTO (2002) standard. This is likely because these specifications recommend the corresponding bending moment distribution factors to compute the maximum stress on bridge superstructures. This indicates a need to develop new equations with which to calculate live load distribution factors for compressive stress, tensile stress and deflection that are closer to the actual values.

8 Empirical Formulae for the Stresses and the Deflection

Samaan et al. (2002a) obtained the following empirical formulas for the maximum positive ($D\sigma_{p, sb}$) and negative (compression) distributions of stress ($D\sigma_{n, sb}$), and for the deflection distribution factor ($D\delta_{s, sb}$) for steel spread open box girder bridges:

$$D\sigma_{p, sb} = \frac{1.35 \times N_L^{0.65}}{N_B \times L^{0.06}} \tag{5}$$

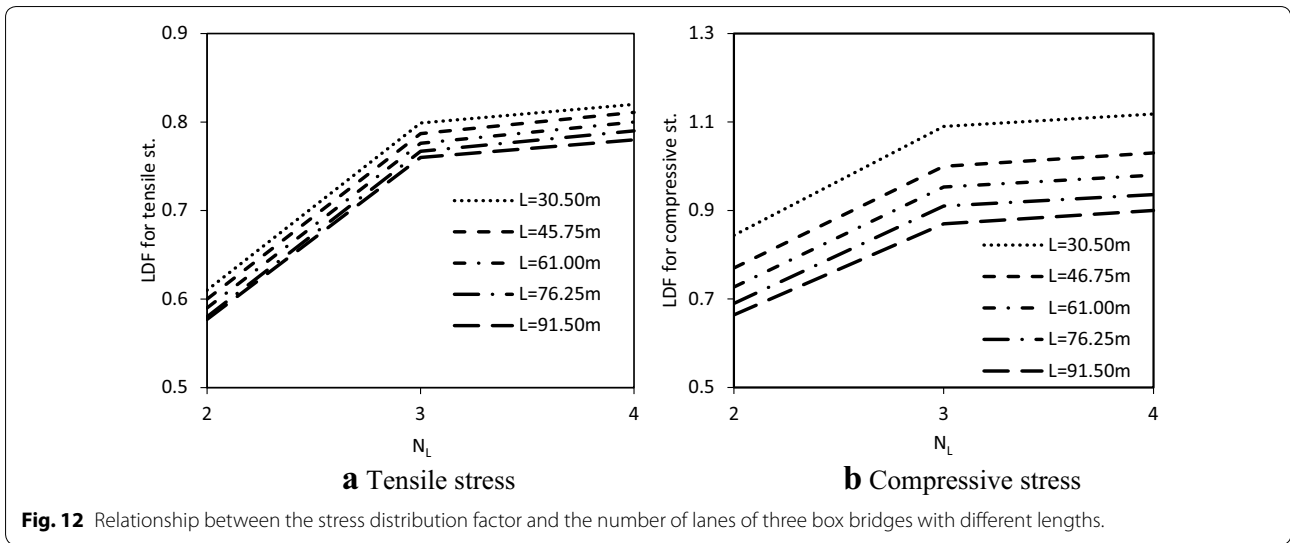


Fig. 12 Relationship between the stress distribution factor and the number of lanes of three box bridges with different lengths.

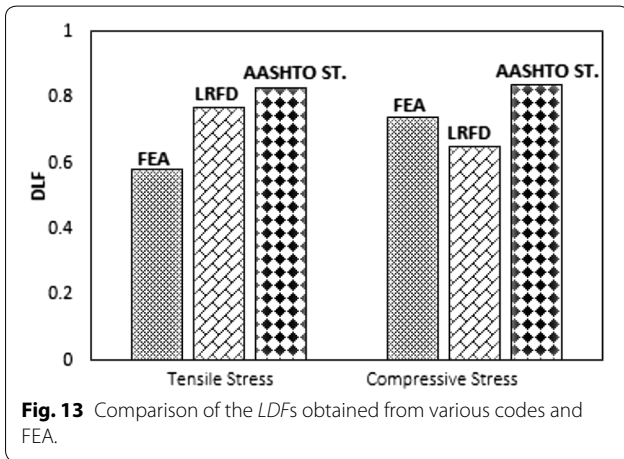


Fig. 13 Comparison of the LDFs obtained from various codes and FEA.

$$D\sigma_{N, sb} = \frac{0.65 \times N_L^{0.7} \times L^{0.06}}{N_B^{0.9}} \tag{6}$$

$$D\delta_{s, sb} = \frac{1.68 \times N_L^{0.65}}{N_B \times L^{0.13}} \tag{7}$$

Since the key parameters determining the stress distribution factor for the two types of superstructure are similar, in this section appropriate correction factors are identified to modify Eqs. (5)–(7) in order to calculate $D\sigma_{po}$, $D\sigma_{ne}$ and $D\delta_s$ for MCB bridges.

8.1 Positive Stress Distribution Factor

To calculate $D\sigma_{po}$ for multicell box girder bridges, the value for $D\sigma_{p, sb}$ obtained from Eq. (5) can be multiplied

by a correction factor (F_p). Hence, the positive stress distribution factor becomes:

$$D\sigma_{po} = F_p \times D\sigma_{p, sb} \tag{8}$$

where

$$F_p = a \times f(L^{b1}, N_B^{b2}, N_L^{b3}) \tag{9}$$

It is assumed that F_p is an exponential function of the form, ax^b , where x is the value of the given parameter and the constants, a , $b1$, $b2$ and $b3$, are obtained via regression analyses using the FEA data. To determine these constants, the ratio of the positive (tensile) stress distribution factor, $R1$, calculated from FEA using Eq. (5) was plotted as a function of the span length (L); the results are shown in Fig. 14a.

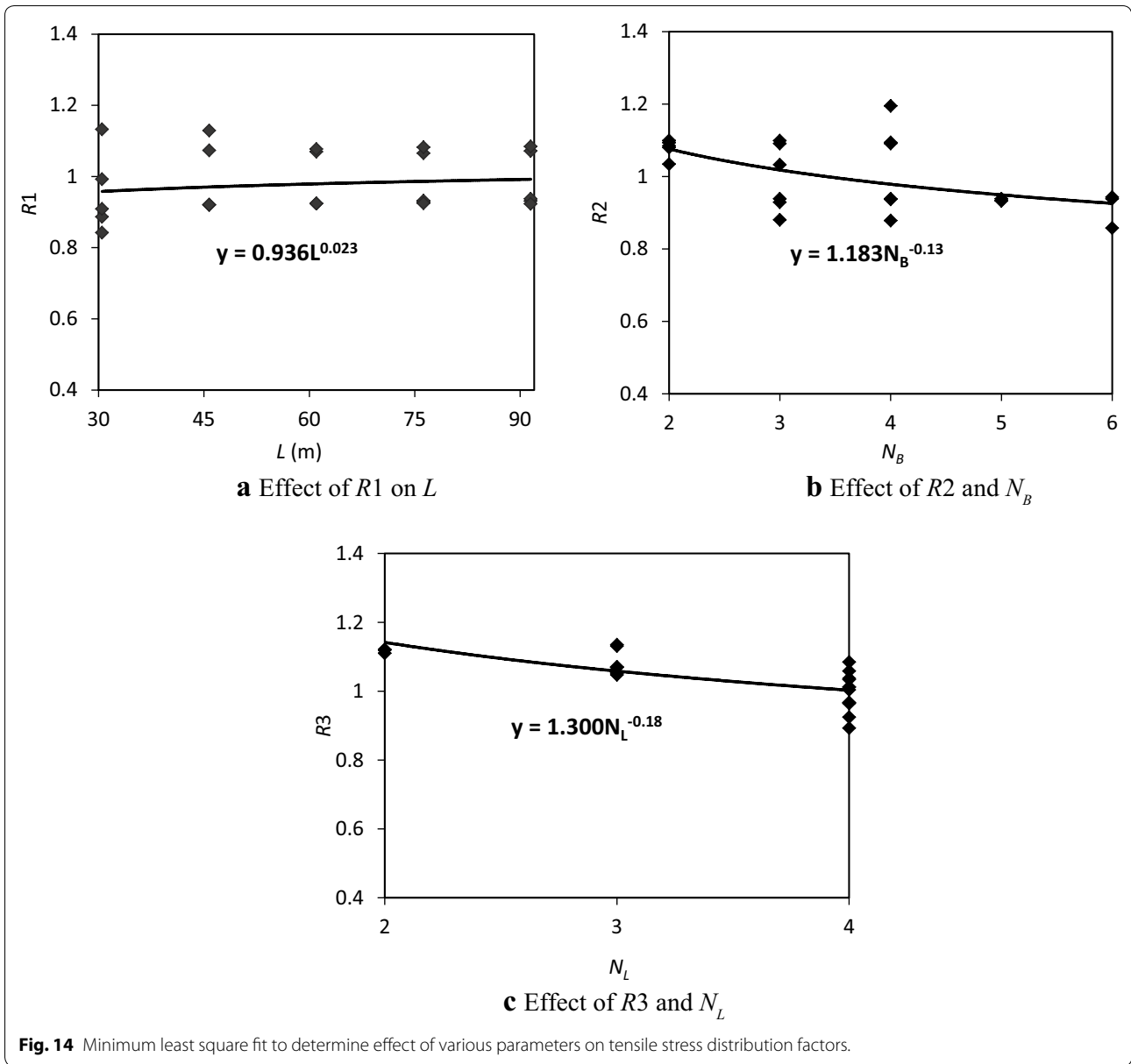
Then, the minimum least square fit of the logarithm of the L - $R1$ data shown in Fig. 14a is carried out to develop the following equation:

$$R1 = 0.936L^{0.023} \tag{10}$$

Equation (10) indicates the ratio of live load distribution factor obtained from FEA to that from proposed equation by Samaan et al. (2002a) as a function of span length. The term $L^{0.023}$ in Eq. (10) represents the term L^{b1} in Eq. (9). Hence, $b1$ is equal to 0.023. The scatter shown in Fig. 14a is due to the absence of the other key parameters, N_B and N_L , in the Eq. (9). In order to remove this error, the effects of these remaining parameters should be taken into account. For this purpose, the ratio of $R2$ is first determined with the following equation:

$$R2 = \frac{D\sigma_{p, FEA}}{R1 \times D\sigma_{p, sb}} \tag{11}$$

where $R2$ indicates the ratio of the positive (tensile) stress distribution factor obtained from the finite element



method to that calculated from Eq. (4) correlated with respect to L . Then, the ratio $R2$ is plotted as a function of the number of boxes, as shown in Fig. 14b. The minimum least square fit of the logarithm of the data shown in Fig. 14b is then carried out to determine Eq. (12).

$$R2 = 1.184 \times N_B^{-0.13} \tag{12}$$

The term $N_B^{-0.13}$ in Eq. (12) is equivalent to the term N_B^{b2} in Eq. (9), so $b2$ is equal to -0.13 . The remaining parameters can be obtained by following a procedure similar to that described above. Then, the parameter $b3$ is calculated as -0.18 using the data shown in Fig. 14c and applying a regression method. Similarly the constant “ a ” in Eq. (9) is obtained as $0.936 \times 1.184 \times 1.30 = 1.44$ by multiplying the

coefficients in front of the variables L , N_B , and N_L calculated following the procedure described above. Equation (13) represents the final form of the correction factor, F_p ;

$$F_p = \frac{(1.81 \times L^{0.023})}{N_B^{0.13} \times N_L^{0.18}} \tag{13}$$

Thus, the proposed equation for the positive (tensile) stress distributions in MCB bridges developed from Eq. (5) becomes:

$$D\sigma_{po} = \frac{2.01N_L^{0.51}}{L^{0.04}N_B^{1.2}} \tag{14}$$

8.2 Negative (Compression) Stress Distribution Factor

To find an equation for the negative stress distribution factor, $D\sigma_{ne}$, for MCB bridges, $D\sigma_{n,sb}$ from Eq. (6) can be multiplied by a correction factor, F_N . This correction factor is assumed to have a form similar to that shown in Eq. (9), so using a similar process to that utilized in the previous section, F_N becomes:

$$F_N = \frac{10.68}{L^{0.25} \times N_B^{0.29} \times N_L^{0.80}} \quad (15)$$

The proposed equation for the negative stress distribution in MCB bridges that is equivalent to Eq. (6) then becomes:

$$D\sigma_{ne} = \frac{5.38 \times N_L^{0.52}}{L^{0.19} \times N_B^{1.19}} \quad (16)$$

8.3 Distribution Factor for Deflection

The distribution factor for maximum deflection, $D\delta_s$, was determined in the same manner as in the previous section for the stress distribution factor. Here, Eqs. (17) and (18) were utilized to calculate the distribution factor, DF , and deflection factor, $D\delta_s$, respectively, for MCB bridges:

$$DF = \frac{4.3}{L^{0.04} \times N_B^{0.25} \times N_L^{0.25}} \quad (17)$$

$$D\delta_s = \frac{7.23 \times N_L^{0.4}}{L^{0.17} \times N_B^{1.25}} \quad (18)$$

9 Verification of the Proposed Equations

The formulae obtained for the stress distribution factors given in Eqs. (14) and (16) and the deflection distribution factor from Eq. (18) were then verified by comparing their outputs against the available FEA results. For this purpose, the distribution factors obtained using the new equations proposed here and those from the FEA and from Eqs. (5)–(7) were plotted as a function of N_L , N_B , and L . The comparison of DF s is shown in Fig. 15. They suggest that Samaan's equations (Samaan et al. 2002a) predict highly unconservative values of positive (tensile) and negative stress distribution factor for the range of values of L , N_B and N_L utilized in this research. However, the new equations proposed here produce reasonable estimates for both the positive (tensile) and negative stress distribution factors for MCB bridges, as demonstrated by the average (AVG) and standard deviation (STD) for the ratio of the proposed equation to the FEA results presented in Table 3. The AVG is almost unity, which indicates that the proposed equations can be used conservatively to predict stress distribution factors,

while the low value for STD indicates that the proposed equations offer a useful approach for predicting the corresponding distribution factors. The values obtained for the coefficients of determination (R^2) of 0.918, 0.934 and 0.968 for the positive (tensile) stress, negative stress and deflection distribution factors, respectively, confirm the acceptably low variability of the data.

10 Applicability of the Proposed Equations for Three and Four-Equal-Span Bridges

The empirical Eqs. (14) through (16) for the various distribution factors were developed taking into account the variations in the span length, number of boxes, and number of lanes. In this section, the applicability of proposed equations for MCB bridge with three and four-equal-spans are assessed, and three box-girder bridges with two, three and four equal-span-length of 45 m were modeled. The distribution factors were determined through dividing the straining action obtained from the FEA by the corresponding straining action determined from the idealized girder as described in Sect. 6. The results for the tensile and compressive stress and the deflection for the selected bridges are compared in Fig. 16. The live load distribution factors remain almost constant irrespective of the number of spans. The fluctuations of less than 2% for both stress and deflection confirm that these factors do not depend on the number of spans if the distribution factors obtained from the adapted equations are applied.

11 Conclusions

Extensive analytical study was undertaken to establish the static characteristics of continued multicell box-girder bridges under vehicle loading conditions. A comprehensive literature review was carried out to set up the basis for this research work. The results of the literature review indicated a lack of adequate expressions to predict the distribution factors for these types of bridges. The distribution factors included in the AAHTO LRFD specifications were derived based on the grillage analogy, which does not accurately represent the complex nature of three-dimensional bridge structures. Given this lack of information, this study developed a new set of equations to calculate these distribution factors for MCB bridges, which would provide a new design methodology for design engineers and code writers seeking to carry out parametric studies for these kind of bridges. Based on the findings of our analytical investigations, the following conclusions can be drawn:

1. The three-dimensional finite element modeling developed herein was verified with results of field and laboratory tests. It was concluded that the adopted modelling method are able to accurately estimate the

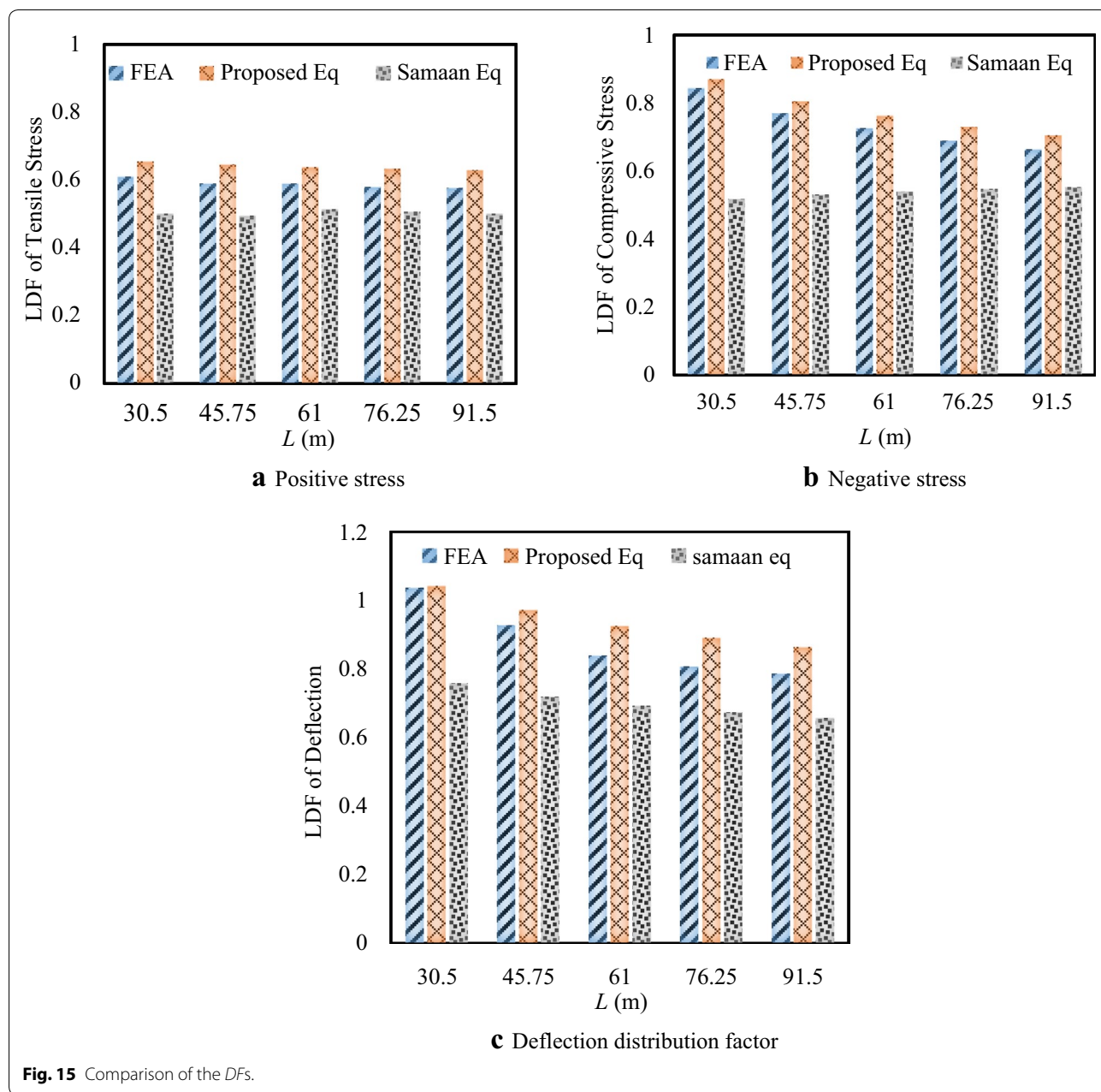


Table 3 Average, standard deviation and variance of the ratios for the DF equations.

Distribution factor (DF)	AVG	STD	Variance
Positive (tensile) stress distribution factor, Eq. (14)	1.0530	0.0640	0.00410
Negative stress distribution factor, Eq. (16)	1.0220	0.0610	0.00380
Deflection distribution factor, Eq. (18)	1.0030	0.0710	0.00500

elastic responses as well as free vibration characteristics such as mode shapes and natural frequencies for the bridges.

2. The live load distribution factor for bending moment of AASHTO (2002) standard and AASHTO LRFD (2017) specifications were reviewed for applicability to MCB bridges. It was revealed that they obtain conservative values for tensile stresses and unconservative values for compressive stresses. Furthermore, these codes are unable to estimate the live load distribution factors for maximum deflection. The newly

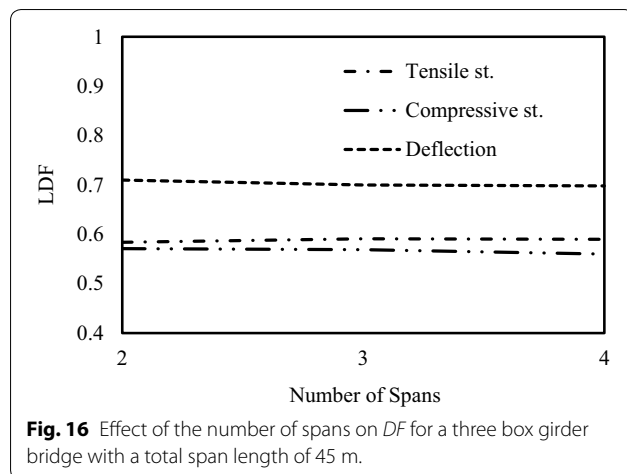


Fig. 16 Effect of the number of spans on DF for a three box girder bridge with a total span length of 45 m.

proposed live load distribution factor equations were developed for tensile and compressive stresses and deflection, which provided conservative results with respect to finite element analysis.

- Based on the results of parametric study, it was concluded that the span length, number of lanes and number of boxes are the most crucial parameters that could affect the load distribution factors of such bridges. The proposed parameters, therefore, were developed as a function of these key parameters.
- Empirical equations were derived for live load distribution factors of maximum tensile stresses at the bottom fiber of box-girders along the span, compressive stresses at the bottom fiber of box-girders at the pier, and deflection along the span of two-equal span MCB bridges. The proposed equations can be applied in the design of equal-span continuous bridges with number of spans up to four. They can be also applicable under AASHTO LRFD truck loading.

Abbreviations

a, b_1, b_2, b_3 : Constants for regression analyses; AVG : Average; B : Width of the boxes; D : Depth of the boxes; d' : Thickness of the top flange; d'' : Thickness of the bottom flange; DF : Distribution factor; DLA : Dynamic load allowance; $D\delta_s$: Distribution factor for maximum deflection; $D\sigma_{ne}$: Distribution factors for the maximum negative stresses; $D\sigma_{n, sb}$: Distribution factors for the maximum negative stresses for steel spread open box girder bridges; $D\sigma_{po}$: Distribution factors for the maximum positive stresses; $D\sigma_{p, sb}$: Distribution factors for the maximum positive stresses for steel spread open box girder bridges; E_c : Modulus of elasticity of the concrete; E_s : Modulus of elasticity of the steel; F_N, F_p : Correction factor; L : Length of the span; L_c : Length of the cantilever; ΣL_i : Sum of all girder actions; LDF : Live-load distribution factor; LDF_i : Live-load distribution factor of the i th girder; LDF_m : Live-load distribution factor of multicell box girder bridges; L_i : Moment or deflection of i th girder; M^- : Maximum negative moment; M^+ : Maximum positive moment; n : Number of bridge girders; N_b : Number of boxes; N_c : Number of boxes; N_L : Lanes of traffic; R_1, R_2 : Ratio of the positive (tensile) stress distribution factor; S : Width of each box; STD : Standard deviation; W_r : Width of the road way of the bridge; W_{total} : Total

width of the bridge; δ_{max} : Maximum deflections; δ : Maximum deflection at the midspan of simple ideal girder; σ_n : Maximum negative (compression) stress for the bridges were then obtained for the three-dimensional bridges using FEA; $\sigma_{n, f}$: Negative (compression) stress at the bottom fiber were calculated using a simple beam bending formula; σ_p : Maximum positive (tensile) stress for the bridges were then obtained for the three-dimensional bridges using FEA; $\sigma_{p, f}$: Maximum positive (tensile) stress at the bottom fiber were calculated using a simple beam bending formula; ν_c : Poisson's ratio of elasticity of the concrete; ν_s : Poisson's ratio of elasticity of the steel.

Authors' contributions

IM performed a numerical study on MCB bridges; JK, WC and JP performed a theoretical study on data collected, and JK and IM suggested simplified methods using proposed equations to deduce proposed expressions for $LDFs$ of MCB bridges. All authors read and approved the final manuscript.

Author details

¹ Department of Landscape Architecture and Rural Systems Engineering, Seoul National University, 1 Gwanak-ro, Gwanak-gu, Seoul 08826, South Korea. ² Department of Civil Engineering, Sangmyung University, Cheonan 31042, South Korea. ³ Research Institute of Agriculture and Life Science, Seoul National University, Seoul 08826, South Korea.

Acknowledgements

The work reported here was supported by Grants (17CTAP-C132629-01, 17CTAP-C132633-01, 18CTAP-C144787-01) funded by the Ministry of Land, Infrastructure and Transport (MOLIT) of the Korean Agency for Infrastructure Technology Advancement (KAIA). This financial support is gratefully acknowledged.

Competing interests

The authors declare that they have no competing interests.

Availability of data and materials

The data used to support the findings of this study are available from the corresponding author upon request.

Ethics approval and consent to participate

For this type of study formal consent is not required.

Publisher's Note

Springer Nature remains neutral with regard to jurisdictional claims in published maps and institutional affiliations.

Received: 12 March 2018 Accepted: 29 January 2019

Published online: 13 March 2019

References

- AASHTO. (2002). *Standard specifications for highway bridges* (17th ed.). Washington, D.C.: American Association of State Highway and Transportation Officials.
- AASHTO LRFD (2014) *LRFD bridge design specifications* (14th ed.) U.S.: American Association of State Highway and Transportation Officials, National Academy of Sciences National Research Council.
- AASHTO. (2017). *LRFD bridge design specifications* (8th ed.). Washington D.C.: American Association of State Highway and Transportation Officials, National Academy of Sciences National Research Council.
- Ashebo, D. B., Chan, T. H. T., & Yu, L. (2007). Evaluation of dynamic loads on a skew box girder continuous bridge Part I: Field test and modal analysis. *Engineering Structures*, 29, 1064–1073. <https://doi.org/10.1016/j.engstruct.2006.07.014>.
- Bae, H. U., & Oliva, M. G. (2012). Moment and shear load distribution factors for multigirder bridges subjected to overloads. *Journal of Bridge Engineering*, 17, 519–527. [https://doi.org/10.1061/\(ASCE\)BE.1943-5592.0000271](https://doi.org/10.1061/(ASCE)BE.1943-5592.0000271).
- Barr, P., Eberhard, M., & Stanton, J. (2001). Live-load distribution factors in prestressed concrete girder bridges. *Journal of Bridge Engineering*, 11, 573–581. [https://doi.org/10.1061/\(ASCE\)1084-0702\(2006\)11:5\(573\)](https://doi.org/10.1061/(ASCE)1084-0702(2006)11:5(573)).

- Computers & Structures, Inc. (2017). CSIBridge, version 20. <http://www.csiamerica.com>.
- Deng, Y., & Phares, B. (2016). Automated bridge load rating determination utilizing strain response due to ambient traffic trucks. *Engineering Structures*, 117, 101–117. <https://doi.org/10.1016/j.engstruct.2016.03.004>.
- Deng, Y., Phares, B. M., & Ping, L. (2017). Lateral live-load distribution of dual-lane vehicles with nonstandard axle configurations. *Journal of Bridge Engineering*, 22, 1–14. [https://doi.org/10.1061/\(ASCE\)BE.1943-5592.0001014](https://doi.org/10.1061/(ASCE)BE.1943-5592.0001014).
- Fanous, F., May, J., & Wipf, T. (2010). Development of live-load distribution factors for glued-laminated timber girder bridges. *Journal of Bridge Engineering*, 16, 179–187. [https://doi.org/10.1061/\(ASCE\)BE.1943-5592.0000127](https://doi.org/10.1061/(ASCE)BE.1943-5592.0000127).
- Hall, D. H., Grubb, M. A., & Yoo, C. H. (1999). Improved design specifications for horizontally curved steel girder highway bridges. *NCHRP Report 424. Transportation Research Board*. Washington D.C.: National Academy Press.
- Hays, C. O., Sessions, M., & Berry, A. J. (1986). Further studies on lateral load distribution using a finite element method. *Transportation Research Record*, 1072, 6–14.
- Higgins, C., Turan, T. O., Connor, J. R., & Liu, J. (2011). Unified approach for LRFD live load moments in bridge decks. *Journal of Bridge Engineering*, 16, 804–811. [https://doi.org/10.1061/\(ASCE\)BE.1943-5592.0000217](https://doi.org/10.1061/(ASCE)BE.1943-5592.0000217).
- Hughs, E., & Idriss, R. (2006). Live-load distribution factors for prestressed concrete, spread box-girder bridge. *Journal of Bridge Engineering*, 11, 573–581. [https://doi.org/10.1061/\(ASCE\)1084-0702\(2006\)11:5\(573\)](https://doi.org/10.1061/(ASCE)1084-0702(2006)11:5(573)).
- Huo, X. S., Conner, S., & Iqbal, R. (2003). *Re-examination of the simplified method (Henry's Method) of distribution factors for live load moment and shear*. Final Report, Tennessee DOT Project No. TNSPR-RES 1218, Tennessee Technological University, Cookeville, TN.
- Huo, X., & Zhang, Q. (2008). Effect of skewness on the distribution of live load reaction at piers of skewed continuous bridges. *Journal of Bridge Engineering*, 13, 110–114. [https://doi.org/10.1061/\(ASCE\)1084-0702\(2008\)13:1\(110\)](https://doi.org/10.1061/(ASCE)1084-0702(2008)13:1(110)).
- Li, H. (1992). Thin-walled box beam finite elements for static analysis of curved and skew box girder bridges. Ph.D. Thesis, Department of Civil Engineering, Carleton University Ottawa, Canada.
- Mohseni, I., & Khalim, A. R. (2013). Development of the applicability of simplified Henry's method for skewed multicell box-girder bridges under traffic loading conditions. *Journal of Zhejiang University: Science A*, 13, 915–925. <https://doi.org/10.1590/S1679-78252013000200002>.
- Mohseni, I., Khalim, A. R., & Nikbakht, E. (2014). Effectiveness of skewness on dynamic impact factor of concrete multicell box-girder bridges subjected to truck loads. *Arabian Journal for Science & Engineering*, 8(6083–6094), 97. <https://doi.org/10.1631/jzus.A1200098>.
- Newmark, N. M. (1938). *A distribution procedure for analysis of slabs continuous over flexible beams*. Urbana, IL: University of Illinois.
- Samaan, M. (2004). *Dynamic and static analyses of continuous curved composite multiple-box girder bridges*. Ph.D. Thesis, University of Windsor. Windsor, Ontario, Canada.
- Samaan, M., Sennah, K. M., & Kennedy J. B. (2002a). Distribution of wheel loads on continuous steel spread-box girder bridges. *Journal of Bridge Engineering*, 7(3), 175–183.
- Samaan, M., Sennah, K. M., & Kennedy J. B. (2002b). Positioning of bearings for curved continuous spread-box girder bridges. *Canadian Journal of Civil Engineering*, 29, 641–652.
- Semendary, A., Walsh, K., & Steinberg, E. (2017). Early-age behavior of an adjacent prestressed concrete box-beam bridge containing UHPC shear keys with transverse dowels. *Journal of Bridge Engineering*, 22, 1–14. [https://doi.org/10.1061/\(ASCE\)BE.1943-5592.0001034](https://doi.org/10.1061/(ASCE)BE.1943-5592.0001034).
- Song, S., Chai, Y., & Hida, S. (2003). Live-load distribution factors for concrete box-girder bridges. *Journal of Bridge Engineering*, 8, 273–281. [https://doi.org/10.1061/\(ASCE\)1084-0702\(2003\)8:5\(273\)](https://doi.org/10.1061/(ASCE)1084-0702(2003)8:5(273)).
- Terzioglu, T., Hueste, M. B. D., & Mander, J. B. (2017). Live load distribution factors for spread slab beam bridges. *Journal of Bridge Engineering*, 22, 1–15. [https://doi.org/10.1061/\(ASCE\)BE.1943-5592.0001100](https://doi.org/10.1061/(ASCE)BE.1943-5592.0001100).
- Zheng, L. (2008). *Development of new distribution factor equations of live load moment and shear for steel open-box girder bridges*. Ph.D. dissertation, Tennessee Technological University, Cookeville, TN.
- Zokaie, T. (2000). AASHTO LRFD live load distribution specifications. *Journal of Bridge Engineering*, 5, 131–138. [https://doi.org/10.1061/\(ASCE\)1084-0702\(2000\)5:2\(131\)](https://doi.org/10.1061/(ASCE)1084-0702(2000)5:2(131)).
- Zokaie, T., Mish, K., & Imbsen, R. (1993). *Distribution of wheel loads on highway bridges. Phase 3*. Final Report to National Cooperative Highway Research Program (NCHRP rep. 12–26), Transportation Research Record, Washington D.C.

Submit your manuscript to a SpringerOpen® journal and benefit from:

- Convenient online submission
- Rigorous peer review
- Open access: articles freely available online
- High visibility within the field
- Retaining the copyright to your article

Submit your next manuscript at ► springeropen.com
